Global Environmental Science
www.sciltp.com/journals/ges

*Review*

# Recent Advances in Material-Based Platforms for Rapid Uranyl Detection and Removal

Wentao Zhang [1], Zhenli Sun [1,*], Suhua Wang [2], Xishi Tai [3] and Xiangke Wang [1,*]

[1] MOE Key Laboratory of Resources and Environmental System Optimization, College of Environmental Science and Engineering, North China Electric Power University, Beijing 102206, China
[2] School of Environmental Science and Engineering, Guangdong University of Petrochemical Technology, Maoming 525000, China
[3] College of Chemistry and Chemical Engineering, Weifang University, Weifang 261061, China
* Correspondence: sunliva@ncepu.edu.cn (Z.S.); xkwang@ncepu.edu.cn (X.W.)

**How To Cite:** Zhang, W.; Sun, Z.; Wang, S.; et al. Recent Advances in Material-Based Platforms for Rapid Uranyl Detection and Removal. *Glob. Environ. Sci.* **2025**, *1*(2), 164–179. https://doi.org/10.53941/ges.2025.100014

**Publication History**

Received: 30 August 2025
Revised: 14 November 2025
Accepted: 19 November 2025
Published: 24 November 2025

**Keywords**

uranyl; detection; removal; material; artificial intelligence

**Abstract:** Nuclear energy is a key low-carbon source for global carbon neutrality, yet its rapid expansion has intensified uranium mining, fuel processing, and nuclear wastewater discharge, raising concerns about the environmental and health risks associated with uranyl ($UO_2^{2+}$) contamination. Reliable monitoring and effective removal of uranium contamination are therefore essential for ensuring environmental safety and conducting accurate risk assessment. Advanced material-based sensors have emerged as promising solutions, owing to their high sensitivity, selectivity, portability, and rapid response. Recent advances feature platforms based on noble metals, quantum dots, metal–organic frameworks, covalent organic frameworks, and nanocomposites, which enable efficient uranyl removal and detection through optical, electrochemical, and multifunctional strategies. The integration of artificial intelligence for spectral interpretation and recognition is also discussed, highlighting its potential to overcome challenges in complex water matrices. This review further outlines perspectives on sustainable, field-deployable platforms for uranyl detection and removal, aiming to safeguard environmental health and support effective nuclear wastewater management.

**Highlights**

- Summarized advances in materials-based platforms for uranyl detection
- Highlighted the roles of advanced materials in uranyl removal
- Discussed AI integration and future perspectives in this field

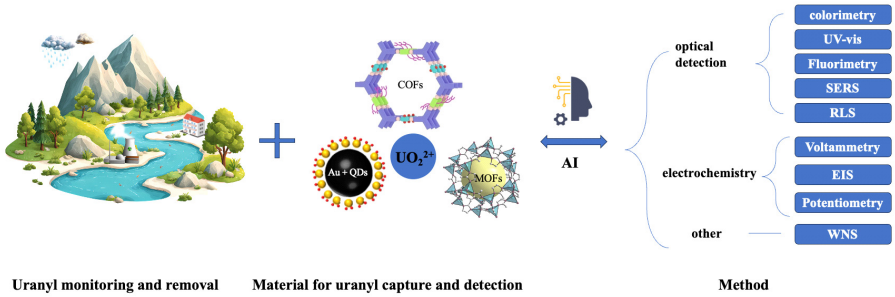


## 1. Introduction

Nuclear energy has been increasingly recognized as a key low-carbon energy source to meet rising global electricity demands while addressing climate change and energy security challenges [1]. With the rapid expansion of the nuclear industry, the demand for uranium resources continues to grow [2]. A large amount of uranium-containing wastewater will be generated and released during mining, milling, purification, reactor operation, laboratory discharge, and accidental leakage [3], lead to the accumulation of uranyl ions ($UO_2^{2+}$) in water and soil systems, posing dual threats due to their radiological hazards and chemical toxicity.

Uranium exhibits multiple oxidation states in the environment, and the most stable and common ionic form in water is the uranyl ion ($UO_2^{2+}$) [4]. Once ingested through contaminated drinking water, uranium can enter the bloodstream via the digestive tract or wounds, subsequently accumulating in the kidneys [5], liver [6], and bones [7], leading to severe health effects. The World Health Organization has therefore set a guideline value of 30 μg/L for uranium in drinking water, highlighting the urgent need for sensitive, selective, and practical detection technologies for both detection and removal [8].

A variety of analytical techniques have been developed for uranium detection, including atomic absorption spectroscopy [9,10], atomic emission spectroscopy [11], X-ray fluorescence [12], mass spectrometry [13], and inductively coupled plasma mass spectrometry [14]. While these laboratory-based approaches provide high sensitivity, their reliance on expensive instrumentation and complex sample pretreatment makes them easily susceptible to interference such as coexisting ions and organic compounds, rendering them unsuitable for real-time and field monitoring. Thus, there is an urgent demand for portable, low-cost, and effective strategies that integrate detection with removal capabilities.

To address this challenge, materials-based platforms, including nanomaterials, metal–organic frameworks (MOFs), and covalent organic frameworks (COFs), have attracted increasing interest due to their large surface areas, tunable functional groups, and strong affinity toward uranyl ions [15,16]. Beyond their widespread use in energy, catalysis, electronics, and biomedical fields, these advanced materials have demonstrated remarkable potential in uranium sensing and remediation, offering rapid response and enhanced sensitivity [17]. Building on these advantages, they have been widely integrated into platforms for uranyl detection and removal. The concept of uranyl sensors has expanded from traditional reversible and continuous-response devices to irreversible probes, enabling rapid, simple, and recyclable detection in environmental and biological systems [18,19].

In recent years, numerous studies have reported uranyl detection–removal platforms, each exhibiting distinct advantages and limitations. Several reviews have summarized the progress in uranyl detection technologies. For instance, He et al. discussed spectral-based sensors (including fluorescence and UV-Vis spectroscopy) for environmental uranyl detection, highlighting molecular probes and recent developments in rapid and sensitive detection [20]. Wu et al. further classified uranyl sensors into optical (e.g., colorimetry and ultraviolet–visible (UV–Vis) spectrophotometry), electrochemical (e.g., voltammetry), and other detection approaches, providing comparative analyses of detection mechanisms, performance parameters, and interference factors [21]. While these studies have significantly advanced the understanding of uranyl sensing mechanisms, most have focused solely on detection technologies and lacked an integrated discussion of material-based platforms that couple detection with removal, as well as the emerging role of artificial intelligence (AI) in data interpretation and material design.

To bridge these gaps, the present review conducts a comprehensive analysis of advanced material platforms for uranyl detection and removal, emphasizing optical and electrochemical strategies. Detection mechanisms, material design concepts, and performance metrics of representative sensors are critically compared to highlight their advantages and limitations. In addition, AI-enabled approaches for spectral interpretation, intelligent pollutant recognition, and data-driven material optimization are discussed to demonstrate their potential in enhancing selectivity and robustness under complex environmental conditions. To systematically map the evolution of this field, a literature survey was performed in the Web of Science database (2004–2025) using the keywords “colorimetry”, “UV–Vis spectrophotometry”, “fluorescence spectroscopy”, “surface-enhanced Raman scattering (SERS)”, “electrochemical methods” (including voltammetry, electrochemical impedance spectroscopy (EIS), and potentiometry), “resonance light scattering (RLS)”, “wireless magnetoelastic sensor (WMS)”, “machine learning”, and “uranium/uranyl”, covering publications up to July 2025. Figure 1a illustrates the publication trends across different detection methods: voltammetry remains the most widely adopted technique, while applications of Raman, fluorescence, and colorimetric approaches have steadily increased in recent years. Figure 1b presents the distribution of advanced materials used in uranyl sensing, indicating an increasing shift toward nanostructured composites and porous framework materials.

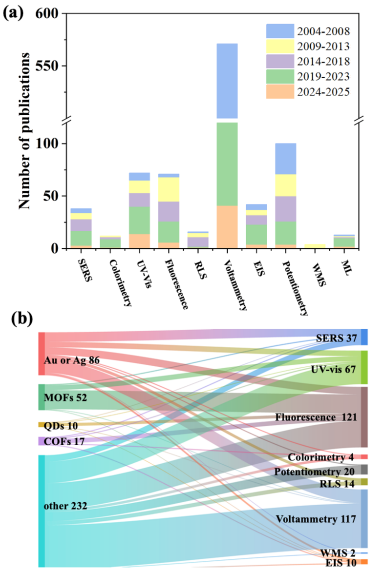


**Figure 1.** (**a**) Publication trends from 2004 to 2025 in uranyl sensor technologies. (**b**) Composition of advanced materials applied across different uranyl detection platforms.

## 2. Rapid Analytical Methods for Uranium Detection

Recent progress in uranyl sensing has been driven by the development of rapid analytical techniques, particularly optical and electrochemical modalities. Compared with conventional laboratory-based assays, these approaches reduce instrumentation demand and sample pretreatment, making them more suitable for field monitoring. Table 1 summarizes representative sensing techniques and their main advantages and limitations. Sections 2.1–2.3 further discuss optical, electrochemical, and other sensor types, highlighting how assay configuration and signal transduction determine sensitivity, selectivity, and robustness.

**Table 1.** Summary of representative rapid sensing techniques for uranyl detection.

| Category | Method | Advantages | Limitations | Refs. |
|---|---|---|---|---|
| Optical Detection | Colorimetry | Simple, low-cost, visual readout; rapid on-site testing | Subtle color differences hard to resolve; lower accuracy | [22,23] |
| | UV–Vis | Fast, low maintenance; non-destructive; economical | Interferences in complex matrices | [24] |
| | Fluorescence | High sensitivity/selectivity; rapid, non-destructive | Photobleaching; dye toxicity; matrix quenching | [20,25] |
| | SERS | Ultrahigh sensitivity; spectral fingerprinting; fast and non-invasive | Gap between lab and field performance; substrate reproducibility | [26–28] |
| | RLS | Simple, fast, sensitive | Aggregation control; matrix effects | [29,30] |
| Electrochemical Sensors | Voltammetry | High sensitivity; in situ and portable | Competing redox species; pretreatment may be required | [31,32] |
| | EIS | Non-destructive; sensitive to interfacial processes | Model dependence; surface stability | [33] |
| | Potentiometry | Low cost; short response; broad range | Detection limit/ion selectivity vary | [34] |
| Other Methods | WMS | Remote, wireless query; portable deployment | Device integration/matrix coupling | [35] |

### *2.1. Optical Detection*

#### 2.1.1. Colorimetric

Colorimetric assays are widely used for uranyl ion ($UO_2^{2+}$) detection because of their simplicity, low cost, and direct visual readout, making them suitable for on-site monitoring [36]. The sensing principle is based on the selective coordination of $UO_2^{2+}$ with designed probes, leading to a distinct color change whose intensity correlates with analyte concentration. However, conventional colorimetric methods suffer from limited sensitivity and selectivity, are susceptible to pH variations [37], and can be interfered by coexisting ions [38–40], which restrict their applicability in complex matrices.

Nanomaterial-based strategies, particularly noble metal nanoparticles (AuNPs, gold nanoparticles; AgNPs, silver nanoparticles), have significantly advanced this field. These probes exploit color transitions induced by surface plasmon resonance (SPR) between dispersed and aggregated states, providing powerful probes. For instance, Saha et al. reported a 3-mercaptopropionyl amidoxime-functionalized AuNP sensor with a visual detection limit of detection（LOD） of 0.3 ng/mL, though requiring strict pH control [41]. Zhang et al. coupled vinylphosphonic acid functionalized AuNPs (VPA-AuNP) probes with smartphone-based image analysis [42]. The VPA-AuNP probes do not require complex modifiers or pH adjustment, and under optimized conditions, they exhibit selectivity toward 10 types of heavy metal ions. enabling quantitative detection of $UO_2^{2+}$ with a LOD of approximately $2.0 \times 10^{-6}$ mol/L.

Beyond noble metal nanoparticles, nanozyme-based systems have further broadened the toolbox for uranyl sensing. Xu et al. designed a sulfone-based COFs (TAS-COF) that mimics peroxidase activity under visible light, catalyzing 3,3′,5,5′-tetramethylbenzydine (TMB) oxidation [43]; the introduction of $UO_2^{2+}$ suppressed the reaction, establishing a “signal-off” mode. Meanwhile, TAS-COF exhibited optimal oxidase-like activity at pH 3.5 (Figure 2a). Except for UO, no significant color change or absorbance fluctuation was observed after the addition of other interfering ions, indicating that this colorimetric sensing system has good specificity for the determination of $UO_2^{2+}$ (Figure 2b). In contrast, Xiao et al. utilized a donor–acceptor structured COF [44], where $UO_2^{2+}$ enhanced catalytic activity, producing a yellow readout in a “signal-on” format.

Despite these advances, real-world applications still require improved anti-interference capability, robustness, and long-term stability. Future directions include the design of highly selective ligands, surface-engineered nanoprobes, and hybrid multimode sensing platforms (e.g., colorimetric–fluorescence). Integration with portable devices such as smartphones and

 https://doi.org/10.53941/ges.2025.100014

miniaturized spectrometers will further accelerate their practical deployment in environmental surveillance and nuclear safety monitoring.

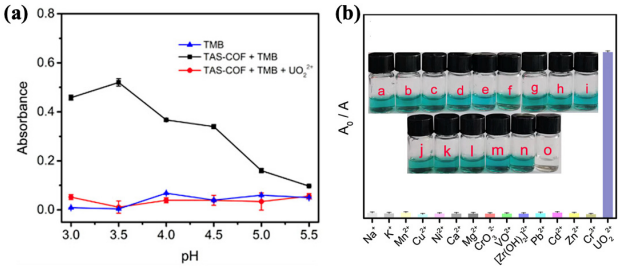


**Figure 2.** (**a**) Effect of pH on the absorbance at 650 nm for TMB, TAS-COF + TMB, and TAS-COF + TMB + $UO_2^{2+}$ under visible-light irradiation. (**b**) Selectivity toward $UO_2^{2+}$ over other interfering ions [43]. Reprinted with permission from Ref. [43]. Copyright 2022, MDPI.

### 2.1.2. UV–Vis

UV–Vis is one of the most established techniques for uranyl determination and has been incorporated into several national standard protocols due to its simplicity, low cost, and reliability. In conventional practice, the method quantifies the absorbance of uranyl–ligand complexes in the UV–Vis region. However, its performance is often limited by insufficient sensitivity and selectivity, particularly in complex environmental matrices where coexisting ions interfere.

To address these limitations, noble metal nanoparticles have been employed to enhance UV–Vis detection. Zhang et al. developed a VPA–AuNPs system, achieving a LOD of 1.07 × $10^{-6}$ mol/L, Compared with the LOD of the naked-eye observation method (2.0 × $10^{-6}$ mol/L) [42], this represents a significant reduction in the LOD. This result demonstrates that UV–Vis, when coupled with nanomaterials, can deliver sensitivities suitable for trace-level monitoring.

Recent studies further emphasize the role of composite and hybrid materials in boosting both sensitivity and selectivity. Amini et al. reported a GO/$Fe_3O_4$/$OPO_3H_2$/PCN-222 composite [45], which combined adsorption with spectroscopy to achieve a LOD of 0.9 μg/L and an adsorption capacity of 416.7 mg/g. Building on this concept, Bai et al. designed TpDb-AO@$Fe_3O_4$ magnetic adsorbents [46], where amidoxime-functionalized COFs were integrated with magnetic separation, enabling a broad linear range of 10–200 μg/L. These advances indicate that UV–Vis remains a benchmark technique for uranyl determination. Coupling with nanomaterials and hybrid systems has effectively pushed detection limits to environmentally relevant levels while improving selectivity. The ongoing trend is toward tailored composites that combine adsorption, separation, and spectroscopic readout, paving the way for more robust field applications.

### 2.1.3. Fluorescence Spectroscopy

Fluorescence spectroscopy has attracted attention for uranyl detection owing to its high sensitivity, rapid response, and adaptability for real-time monitoring. Conventional organic dyes (e.g., rhodamine, fluorescein, anthocyanin) have been widely employed, but issues such as low absorption coefficients, photobleaching, and phototoxicity (e.g., FITC generating reactive oxygen species) limit their applicability in continuous monitoring. These drawbacks have motivated the development of nanostructured probes with enhanced brightness, photostability, and biocompatibility.

Fluorescent nanomaterials can be broadly categorized into two types. Metal nanoclusters (NCs, <2 nm, e.g., Au, Ag, Cu, Pt) offer strong luminescence, tunable emission, and facile surface functionalization [47]. Semiconductor quantum dots (QDs, <10 nm) exhibit broad absorption, narrow size-dependent emission, and strong photostability; cadmium chalcogenide QDs are the most studied. In addition, diverse materials such as AuNPs [38], semiconducting nanocrystals [48], MOFs [49,50], polydopamine nanoparticles [51], and carbon-based nanomaterials [52] have expanded the toolkit for uranyl detection, although issues such as synthetic complexity, high cost, and limited sensitivity remain.

Representative advances highlight the potential of nanostructured fluorescence platforms. Zheng et al. developed dopamine-modified $MoO_x$ QDs (Figure 3a) [53], where oxygen- and nitrogen-containing groups on the surface enhanced the specific interaction with $UO_2^{2+}$, inducing the aggregation of QDs and thereby causing fluorescence quenching. This system improved sensitivity nearly 1000-fold compared with pristine $MoO_x$ QDs, achieving a LOD of 3.85 nM. Notably, the platform maintained high selectivity even in complex ion-rich environments with ethylenediaminetetraacetic acid masking. Ghosh et al. synthesized Ce-ATP coordination polymer nanoparticles that reversibly encapsulated thioflavin-T [54], enabling the formation of a stimuli-responsive system with modulated photophysical properties, producing a fluorescence “turn-on” response upon $UO_2^{2+}$ binding. This sensor achieved a LOD of 80 ng/mL, operated over a 0–20 μM range, and directly quantified uranium in seawater without pretreatment. Chen et al. developed a rapid detection method for uranyl ions using dual QDs (MPA@CdTe QDs) based on ratiometric fluorescence signals (Figure 3b) [55]. Uranyl ions significantly quench the red fluorescence of CdTe QDs while the green fluorescence remains stable, resulting in distinct color changes. Based on this principle, a smartphone application and 3D-printed accessories were developed to capture fluorescence signals from test strips immobilized with probes, enabling quantitative analysis and calculation of uranyl ion concentrations. Wang et al. synthesized a novel fluorescent sensor TPE-EDC, by

reacting EDC and TPE-$(COOH)_4$ [56]. Owing to its aggregation-induced emission and intramolecular charge transfer properties, the sensor exhibits high sensitivity and selectivity for uranyl ions, with a LOD as low as 69 pmol/L.

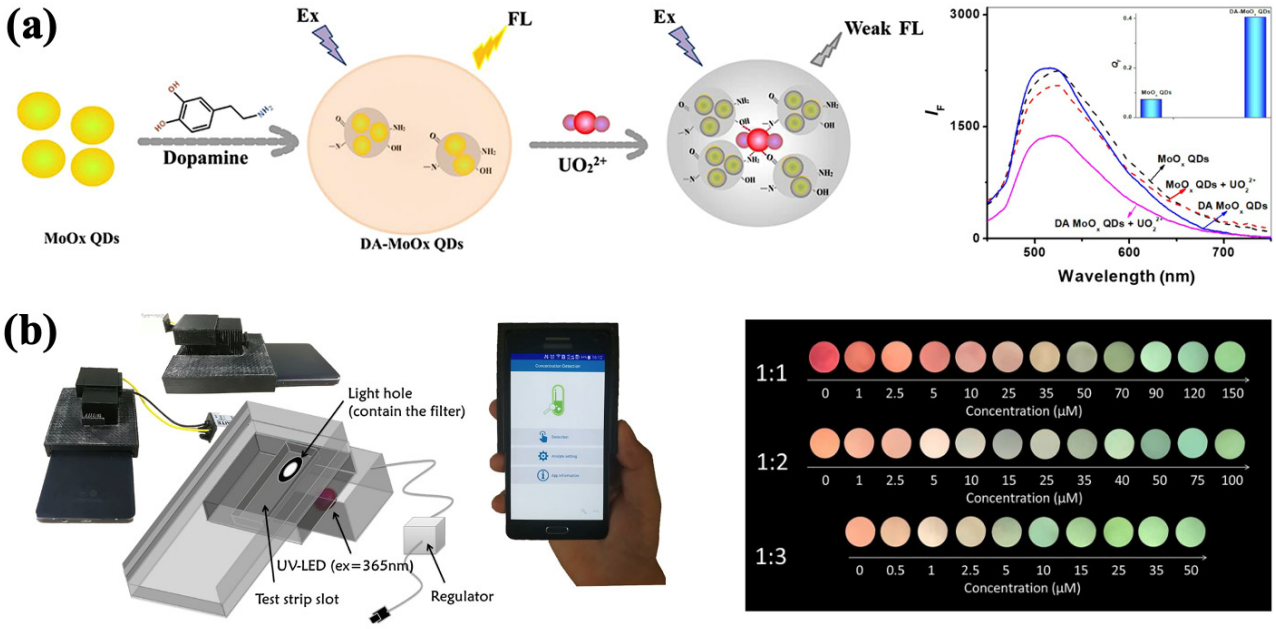


**Figure 3.** (**a**) Schematic of uranium detection using DA-MoOx QDs and fluorescence responses of DA-MoOx QDs and MoOx QDs after incubation with 1 μM $UO_2^{2+}$, reprinted with permission from Ref. [53]. Copyright 2022, Wiley. (**b**) Photograph and structure of the smartphone based platform device for uranyl detection, reprinted with permission from Ref. [55]. Copyright 2018, American Chemical Society.

Compared with other detection methods, fluorescence spectroscopy provides superior sensitivity, rapid response, and practical adaptability. However, research in this area remains relatively limited. Challenges include insufficient stability under extreme conditions, interferences from competing actinides, and material cost issues. Future efforts should focus on developing robust, low-cost nanoprobes with enhanced selectivity and matrix tolerance, facilitating portable and reliable uranium monitoring in complex environments.

### 2.1.4. SERS

SERS has emerged as one of the most promising analytical tools for uranyl detection, owing to its ultrahigh sensitivity and molecular fingerprinting capability. The signal enhancement mainly arises from two mechanisms: (i) electromagnetic enhancement via localized surface plasmon resonance (LSPR) in nanostructured metals such as Ag, Au, and Cu [57,58]; and (ii) chemical enhancement through charge transfer between the substrate and analyte. Current research primarily emphasizes rational substrate design and material functionalization to improve sensitivity, stability, and selectivity.

Substrate design strategies have largely focused on generating dense "hotspots" with metallic nanostructures (e.g., AgNPs, AuNPs), and engineering hybrid architectures to balance sensitivity and stability. Representative examples include $Ag^+$/sodium alginate hydrogels [59] and Ag/$Ag_2O$–COFs [60], which combined plasmonic activity with high surface area porosity, The LOD are 6.7 × $10^{-9}$ mol $L^{-1}$ and 8.9 × $10^{-10}$ mol $L^{-1}$, respectively. The Ag/$Ag_2O$–COF composite achieves such a low LOD because it combines the strong SERS effect of uranyl adsorbed on the Ag/$Ag_2O$ composite with the high adsorption efficiency of COF TpPa-1, thereby enabling the trace detection of uranyl ions. Similarly, $HfO_2$-coated tilted Ag nanorod arrays improved stability while retaining strong enhancement, achieving an LOD of 8.33 ppb [61].

In parallel, surface functionalization has been widely adopted to enhance uranyl enrichment and selectivity. Functional ligands such as carboxyl, amidoxime, and phosphonate improve binding affinity, while bio-inspired and multimodal strategies extend detection capability. For example, pH strongly influences uranyl adsorption, as demonstrated by $Al_2O_3$-coated Ag nanorods, which retained nanomolar sensitivity under acidic/alkaline conditions but performed poorly in neutral media [62]. Functionalized platforms further advanced performance: A DNAzyme/ZnO–Ag microfluidic chip achieved an exceptional LOD of 3.71 × $10^{-15}$ mol/L [63]. This performance is attributed to the three-dimensional ZnO-Ag nanostructure providing a large specific surface area and "hot spots", while the DNAzyme exhibits specific responsiveness to uranyl ions, enabling the precise

 https://doi.org/10.53941/ges.2025.100014

release of signal probes through cleavage reactions. MOF-based composites such as FA@ZIF-8 (Figure 4) further enhanced both preconcentration and separation[64]. In addition, $Fe_3O_4$–Au@CdTe hybrids integrated SERS with fluorescence, enabling simultaneous qualitative and quantitative analysis [65].

Despite remarkable advances, the sensing performance of SERS substrates for uranyl ions remains highly variable, largely dependent on nanostructure design, surface chemistry, and measurement conditions. While some systems achieve nanomolar to femtomolar sensitivity, issues of reproducibility, stability, and matrix interference remain unresolved. To provide a direct comparison, the detection limits and linear ranges of representative substrates are summarized in Table 2, highlighting both the progress achieved and the persistent challenges to be addressed for developing robust, field-deployable SERS platforms for uranium monitoring.

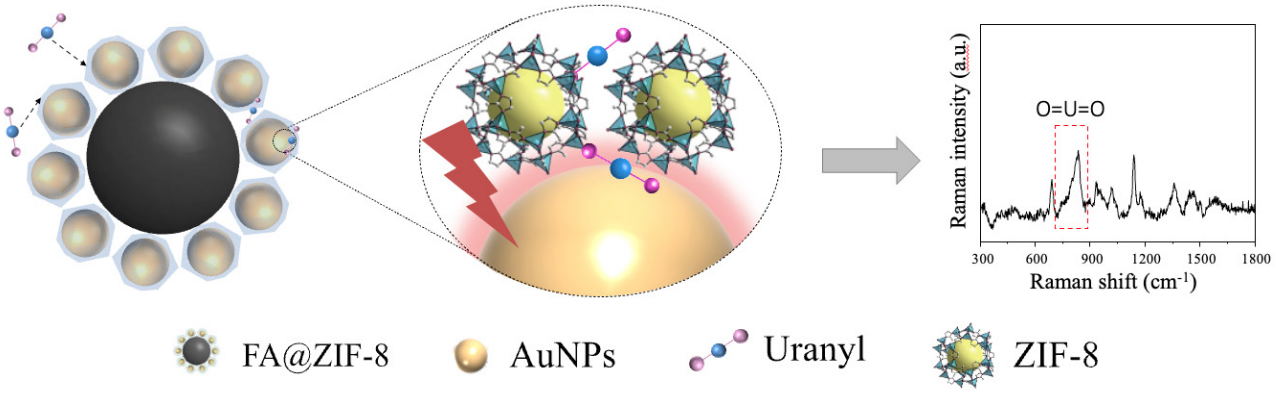


**Figure 4.** Uranyl ion detection based on the FA@ZIF-8 composite SERS substrate, reprinted with permission from Ref. [64]. Copyright 2023, American Chemical Society.

**Table 2.** Performance of representative SERS substrates for uranyl detection.

| Substrate | Characteristic Peak ($cm^{-1}$) | LOD (M) | Linear Relationship (M) | Year | Refs. |
|---|---|---|---|---|---|
| AgNR@$Al_2O_3$ | 720,828 | $2.3 \times 10^{-9}$ | $10^{-9}$–$10^{-7}$ | 2017 | [62] |
| Ag-Si substrate | 720 | $10^{-7}$ | $10^{-7}$–$10^{-3}$ | 2017 | [66] |
| Citrate-stabilized AgNPs | 750 | $6 \times 10^{-8}$ | $2 \times 10^{-7}$–$5 \times 10^{-7}$ | 2018 | [67] |
| $HfO_2$ | 811 | $3.1 \times 10^{-8}$ | $10^{-7}$–$10^{-6}$ | 2018 | [61] |
| ZnO-Ag MNS | 1650 | $3.71 \times 10^{-15}$ | $10^{-13}$–$10^{-7}$ | 2019 | [63] |
| $Fe_3O_4$-Au@CdTe | 828 | $10^{-6}$ | - | 2020 | [65] |
| FA@ZIF8 | 829 | $10^{-7}$ | - | 2023 | [64] |
| Ag/$Ag_2O$–COF | 705–715 | $8.9 \times 10^{-10}$ | $10^{-8}$–$10^{-6}$ | 2024 | [60] |
| Ag/SA SMH | 715 | $6.7 \times 10^{-9}$ | $10^{-8}$–$2 \times 10^{-6}$ | 2024 | [59] |
| Au@ZIF-8 | 828 | $5 \times 10^{-7}$ | - | 2024 | [68] |

### 2.1.5. RLS

RLS is a rapid and sensitive optical technique that has been increasingly applied $UO_2^{2+}$ detection [69]. The detection principle is mainly based on molecular binding or nanoparticle aggregation, which induces changes in the system volume and subsequently enhances the scattering signal. Among them, plasmonic nanomaterials (e.g., AuNPs and AgNPs) are particularly suitable due to their LSPR effect, which produces strong scattering signals at specific wavelengths, thus offering an ideal platform for sensitive sensing [70].

Recent advances have centered on functionalized nanostructures as recognition elements. Zhou et al. developed a DNAzyme–AuNP system [29], where $UO_2^{2+}$ triggered strand cleavage released short duplex DNA, leading to the aggregation of AuNPs and the increase in RLS intensity, yielding a LOD of $4.09 \times 10^{-9}$ mol/L with a linear range of $1.36 \times 10^{-8}$–$1.50 \times 10^{-7}$ mol/L. However, DNAzyme susceptibility to nuclease degradation has motivated the use of more robust ligands. For example, uranyl-specific aptamers (UApt) enabled a label-free UApt–AuNP platform with a LOD of 6.7 nM [71]. Despite these promising results, RLS for uranyl detection still faces challenges in improving probe stability, reducing matrix interference, and achieving portable integration. Addressing these issues will be essential for advancing RLS from proof-of-concept studies to practical uranium monitoring in environmental systems.

## *2.2. Electrochemical Sensors*

Electrochemical sensing provides a versatile platform for $UO_2^{2+}$ detection, combining low-cost instrumentation, simple sample preparation, high sensitivity, and portability [32,72]. Depending on the variations in electrical signals, such as current, voltage, or impedance, these sensors are

typically categorized into voltammetric, impedimetric, and potentiometric methods.

### 2.2.1. Voltammetry

Voltammetric detection relies on the electrochemical response arising from uranyl–electrode interactions. Traditional voltammetry often suffers from insufficient sensitivity, but nanostructured electrode modification has significantly advanced the field. Conductive polymers, carbon nanomaterials, and ion-imprinted systems have been widely used to enhance preconcentration and selectivity. For instance, a poly(nile blue)-modified glassy carbon electrode coupled with differential pulse adsorptive stripping voltammetry achieved an LOD of 0.19 $\mu g \cdot L^{-1}$ [73]. Herein, PNB exhibits excellent conductivity, which accelerates electron transfer on the electrode surface and reduces charge transfer resistance. Similarly, Ghoreishi et al. reported a Schiff base-modified carbon paste electrode and its carbon nanotube composite [74], further reducing the LOD to 0.206 $nmol \cdot L^{-1}$. Likewise, an ion-imprinted graphene oxide-modified carbon paste electrode offered excellent selectivity with an LOD of 1.32 nM [75].

Among voltammetric techniques, differential pulse adsorptive stripping voltammetry (DPAdSV) stands out for its preconcentration–stripping mechanism, enabling both trace detection and quantitative analysis. For example, Zhou et al. [76] employed a GCE in combination with copper–iron reagents and diphenylguanidine as synergistic agents, extending the linear range to 3–80 $\mu g \cdot L^{-1}$. Voltammetry delivers ultralow detection limits through efficient preconcentration, but electrode fouling and matrix interference still hinder its practical deployment.

### 2.2.2. EIS

EIS is a nondestructive technique that probes the impedance of the electrode–electrolyte interface under small alternating perturbations. By sweeping the frequency of an applied sinusoidal signal, EIS reveals charge-transfer and mass-transport processes, in which changes in phase and amplitude can be directly linked to specific ligand–analyte interactions.

In uranyl sensing, EIS has been applied both as a detection tool and as a mechanistic probe. Zhou et al. integrated EIS with DPAdSV to evaluate a poly(nile blue)-modified glassy carbon electrode [73]. By optimizing electrode fabrication and detection parameters, they achieved sensitive analysis with a LOD of 0.19 $\mu g \cdot L^{-1}$. This study demonstrated that EIS not only enhances detection sensitivity but also serves as a powerful tool to investigate the microstructural and transport properties of porous electrode materials. In another study, Wen et al. demonstrated the versatility of EIS by applying it to characterize a Z-scheme photocatalytic system for U(VI) degradation [77].

EIS thus serves a dual role in uranyl research, enabling sensitive detection when integrated with advanced electrode architectures while simultaneously providing mechanistic insights into interfacial charge-transfer processes. Key challenges remain, particularly the reliance of data interpretation on equivalent-circuit modeling and the limited validation of EIS performance under realistic environmental conditions.

### 2.2.3. Potentiometry

Potentiometric methods measure the potential difference between electrodes in the absence of current, offering a straightforward and selective approach for ion analysis. In uranyl sensing, Guo et al. employed potentiometric titration to investigate the complexation behavior of U(VI) with benzoate ions in aqueous solution [78]. Three complexes ($UO_2L^+$, $UO_2L_2$, and $UO_2L_3^-$, where L denotes the benzoate ligand) were identified over the temperature range of 298–343 K, providing crucial insights for predicting the environmental chemical behavior of U(VI). Xie et al. explored the complexation reaction between Mn(II) and glutamic acid dihydrazide, revealing that the process was jointly driven by enthalpic and entropic contributions [79]. This work was further supported by calorimetric and electrochemical measurements, confirming the thermodynamic characteristics of the interaction. Akl et al. developed a triazole-derivative-based potentiometric electrode for the detection of uranyl ions in aqueous media [80]. The electrode, fabricated via the self-assembly of triazole derivatives on silver nanoparticles, exhibited remarkable potentiometric response with a LOD as low as $6.1 \times 10^{-10}$ M. Moreover, it demonstrated good thermal stability over 10–60 °C and successfully detected uranyl ions in real water samples. These findings indicate that potentiometry offers simple and highly selective uranyl detection, but compared with voltammetry and EIS, its development has been focused more on fundamental complexation studies than on practical sensor deployment.

## *2.3. Other Methods*

In addition to the above major techniques, other approaches for uranyl detection have also attracted attention. Among them, WMS stands out due to its excellent performance, portability, and remote sensing capability. WMSs are fabricated from Fe–Ni–Mo–B amorphous ferromagnetic alloys, operate based on magnetostrictive effect: when excited by an external alternating magnetic field, the material undergoes mechanical vibrations and emits magnetic flux signals that can be wirelessly detected. Yang et al. proposed a sandwich-type detection strategy [81], in which a salophen receptor was immobilized on the polyurethane-protected sensor surface to capture uranyl ions, while $Fe_3O_4$ nanoparticles coated with phosphorylated

 https://doi.org/10.53941/ges.2025.100014

poly(vinyl alcohol) served as signal amplification tags. By monitoring resonance frequency shifts, this design achieved highly sensitive uranyl detection. This strategy not only retained the advantages of wireless magnetoelastic sensing but also significantly enhanced detection performance through the synergistic effects of specific molecular recognition and signal amplification. The development of such emerging sensor technologies provides new pathways for rapid on-site uranyl detection in complex environments, although further improvements in selectivity and anti-interference capability remain key challenges for future research.

## 3. Advanced Functional Materials in Uranyl Ion Detection and Removal

Advanced functional materials have been extensively employed in uranyl detection, where selective binding sites translate molecular interactions into measurable signals, and their physicochemical versatility also renders them highly effective for removal [82] These organic, inorganic, and hybrid architectures feature tunable porosity, abundant functional groups, and adaptable electronic properties that enable high-capacity adsorption, selective separation, and even catalytic transformation of $UO_2^{2+}$ in complex environments [83,84]. Notably, the structural attributes that enhance sensing sensitivity often simultaneously drive efficient capture, underscoring their dual functionality and highlighting the promise of integrated detection–remediation platforms. In this section, we summarize recent progress across four representative categories: nanoparticles, MOFs, COFs, and other porous frameworks, focusing on their dual roles in uranyl detection and removal.

### *3.1. Nanoparticle*

Nanoparticles have been widely employed in uranyl research due to their high surface-to-volume ratio, ease of functionalization, and distinctive optical/electronic properties. QDs are semiconductor nanocrystals whose size-dependent photoluminescence can be quenched or enhanced by interaction with U(VI). This effect is mainly governed by strong coordination between uranyl ions and surface ligands, leading to perturbation of the quantum confinement states. For example, Wang et al. synthesized nitrogen-doped carbon dots via a plasma-assisted route, which exhibited excellent performance in both pH and uranyl ion sensing [85]. Chen et al. further developed a dual-probe system (MPA@CdTe) combining carbon dots with Cd-based QDs [55], integrated with an application-based platform, achieving uranyl detection across 1–150 μM with a LOD of 0.5 μM. Sun et al. designed a dual-mode sensor by coupling CdTe QDs with magnetic enrichment (FA@CdTe) [65], allowing sensitive detection of $UO_2^{2+}$ in natural seawater with a LOD as low as 1.2 nM. These examples highlight the high specificity and portability of QDs for rapid and cost-effective environmental monitoring.

AuNPs represent another extensively studied class of nanomaterials. Their LSPR properties render them highly responsive to uranyl-induced aggregation or refractive index changes, enabling naked-eye colorimetric sensing. For instance, Zhang et al. reported vinylphosphonic acid-functionalized AuNPs [42], which aggregated in the presence of $UO_2^{2+}$, producing a visible color change that allowed straightforward visual detection in water samples. Beyond colorimetry, AuNPs also serve as effective substrates for SERS. Wang et al. constructed a satellite-like SERS platform by modifying magnetic FS microspheres with AuNPs and further coating them with porous ZIF-8 (FA@ZIF-8) [64], enabling rapid uranyl detection with a LOD of $1 \times 10^{-7}$ M. Thus, AuNP-based systems extend from straightforward visual assays to highly sensitive spectroscopic platforms, balancing accessibility with analytical power.

Although not designed for direct U(VI) removal, nanoparticles can translate molecular interactions into measurable optical or electrochemical signals, thereby serving as sensitive detection probes and mechanistic evaluators. The responsive photoluminescence of QDs and the plasmonic behavior of AuNPs exemplify how these nanoplatforms not only enable portable and highly sensitive uranyl detection, but also provide opportunities to investigate adsorption interactions. In this way, nanoparticle-based systems act as a bridge between practical sensing and removal-oriented material design, complementing sorbent-focused approaches.

### *3.2. MOFs*

MOFs are crystalline porous materials with tunable structures, large surface areas, and abundant pore channels derived from the coordination between metal centers and organic ligands. Their ordered frameworks allow precise functionalization of recognition sites and favorable host–guest interactions, making them highly attractive for radionuclide applications [86]. In uranyl research, the combination of structural tunability and responsive luminescence provides opportunities for both adsorption and sensing [87].

Recent studies have demonstrated that MOFs can be employed for both adsorption and detection of radionuclides by monitoring fluorescence intensity, offering advantages such as high sensitivity, real-time response, short detection time, low cost, operational simplicity, and minimal sample pretreatment [88]. When exposed to external stimuli, many MOFs exhibit luminescence phenomena, where analytes can induce fluorescence quenching or enhancement depending on their concentration [47]. Such tunability, combined with customizable binding sites and adjustable emission

properties, makes luminescent MOFs one of the most promising candidates for radionuclide sensing.

In particular, luminescent MOFs have emerged as promising platforms for uranyl detection, as the fluorescence intensity of the frameworks can be quenched or enhanced by target ions, allowing for rapid, sensitive, and cost-effective signal readout [89]. For example, Sun et al. synthesized a porphyrin-based MOF (Ni-TCPP) using nickel chloride hexahydrate as the nickel source and tetrakis(4-carboxyphenyl)porphyrin as the organic ligand [90]. Ni-TCPP served as a fluorescence probe for the visual detection and removal of uranyl ions in seawater, showing remarkable responsiveness to ultralow concentrations of $UO_2^{2+}$ (16.59 nM) through an efficient fluorescence "turn-on" mechanism. This renders Ni-TCPP one of the most sensitive MOF-based fluorescent sensors reported to date. Similarly, Wang et al. developed a europium-based coordination polymer (CP-1) that selectively detected $UO_2^{2+}$ ions (Figure 5a) [91]. CP-1 exhibited significantly stronger fluorescence quenching efficiency toward $UO_2^{2+}$ compared to other metal cations, with a calculated LOD of 0.011 mM (Figure 5b). The mechanism was attributed to interactions between $UO_2^{2+}$ ions and the polymer ligand, which weakened energy transfer from the ligand to $Eu^{3+}$, leading to fluorescence quenching. Wang et al. report a hydrolytically stable mesoporous terbium(III)-based MOF [49], designated as compound **1** (Figure 5c), which features abundant exposed Lewis basic sites within its framework. The luminescence intensity of this MOF is selectively quenched by uranyl ions, achieving a LOD of 0.9 μg/L in deionized water.

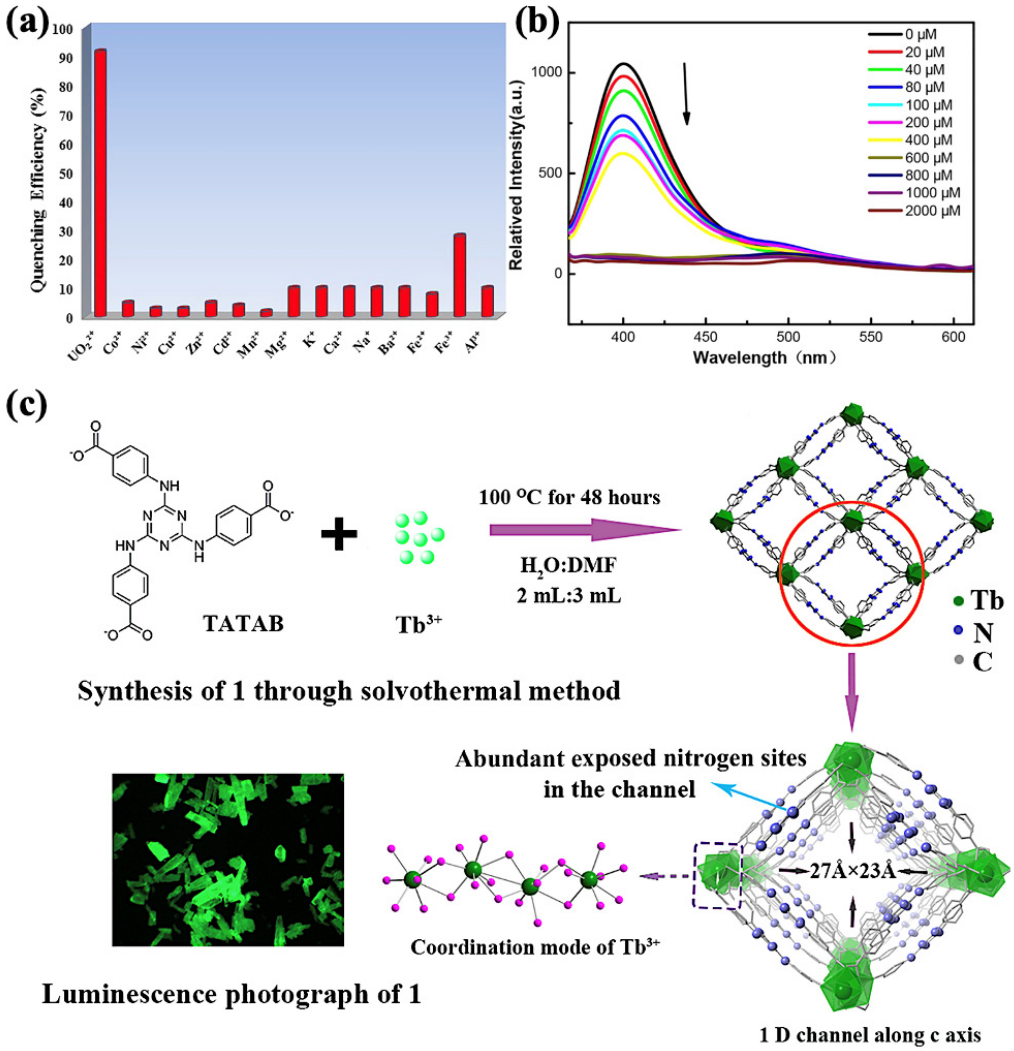


**Figure 5.** (**a**) Comparison of quenching efficiency of CP-1 toward different metal ions and $UO_2^{2+}$, reprinted with permission from Ref. [91]. Copyright 2019, Wiley. (**b**) Fluorescence quenching curves of CP-1 at various uranium concentrations, reprinted with permission from Ref. [91]. Copyright 2019, Wiley. (**c**) Synthesis and crystal structure of mesoporous terbium(III)-based MOF , reprinted with permission from Ref. [49]. Copyright 2017, American Chemical Society.

Cao et al. fabricated an electrochemical sensor dedicated to the detection of uranium [92]. PtRu bimetallic nanoparticles (PtRu bimetallic NPs) were successfully synthesized using MOF-derived porous

carbon (PtRu–PCs) as the support matrix. Among the developed composites, the sensor based on $Pt_1Ru_2$-PC exhibited outstanding electrochemical performance for $UO_2^{2+}$ detection, with a LOD as low as 0.024 μM. The remarkable enhancement in its electrochemical properties is attributed to the synergistic effect between the PtRu nanoparticles and the MOF-derived porous carbon. Notably, this sensor can be directly applied for the accurate determination of uranium (VI) ions in real water samples, demonstrating its practical applicability in environmental monitoring. These studies highlight MOFs as highly promising platforms for uranyl ion detection and removal. Their ordered porous structures provide abundant active sites for selective adsorption, while tunable frameworks allow targeted recognition of $UO_2^{2+}$ with high sensitivity and stability. At the same time, the coupling of adsorption capacity with luminescent readouts underscores their dual functionality, bridging mechanistic understanding with practical sensing applications. Nonetheless, challenges such as high synthesis costs and signal interference from coexisting ions or natural organic matter remain obstacles to large-scale or field deployment.

### *3.3. COFs*

COFs are crystalline porous polymers constructed from light elements such as C, O, and N, interconnected through robust covalent bonds including C=N, C=C, O–C–O, and N–O. Their highly ordered two- or three-dimensional architectures endow them with excellent physicochemical stability, tunable functionalities, and flexible topological design, which have facilitated extensive applications in catalysis, gas storage, and metal ion enrichment. In uranyl research, COFs combine large surface areas with customizable functional groups, offering both high-capacity adsorption and fluorescence-based detection.

Recent studies illustrate the potential of fluorescent COFs. Niu et al. developed a fluorescent COF, TFPPy-BDOH, by incorporating biphenyldiamine and pyrene units into a π-conjugated framework [93]. Specific coordination between imine nitrogen atoms and hydroxyl groups within the conjugated skeleton endowed TFPPy-BDOH with selective binding to $UO_2^{2+}$. This material exhibited an impressive adsorption capacity of 982.6 ± 49.1 mg $g^{-1}$, rapid fluorescence response within 2 s, and a LOD of 8.8 nM, while also demonstrating good regenerability. These properties allowed TFPPy-BDOH to overcome severe interference and achieve precise $UO_2^{2+}$ recognition. Similarly, Zhen et al. developed an amidoxime-modified product (GC-TFPB-AO) [94], which, relying on the synergistic effect of multifunctional groups, enables rapid fluorescent and smartphone-based detection of uranyl ions and exhibits excellent recovery performance (Figure 6).

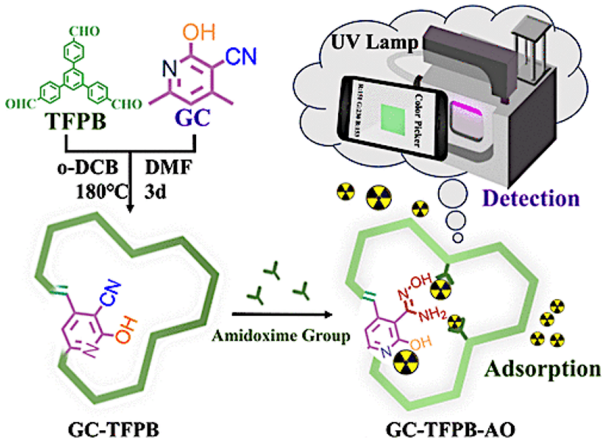


**Figure 6.** Schematic illustration of the synthesis and detection process of GC-TFPB-AO, reprinted with permission from Ref. [94]. Copyright 2024, American Chemical Society.

To develop a substrate with enhanced stability, selectivity, and sensitivity, Guo et al. fabricated a novel SERS substrate (Ag@COF-TpDb-AO) by depositing AgNPs onto amidoxime-functionalized ketoenamine-based COFs [95]. This substrate exhibits a LOD of 3.72 μg/L for uranium, along with a high enhancement factor of $1.26 \times 10^6$, as well as excellent anti-interference ability, reproducibility, and stability. Chen et al. further developed an innovative colorimetric-electrochemical dual-mode sensor specifically designed for $UO_2^{2+}$ detection [96]. Constructed with the AuNCs@COF composite as its core, the sensor benefits from the incorporation of AuNCs, which not only endows the composite with excellent peroxidase-like catalytic activity but also enhances its electrochemical performance. By regulating the adsorption and desorption behaviors of aptamers on the surface of AuNCs@COF, the peroxidase-like activity and conductivity of the composite can be synchronously modulated, thereby enabling the accurate detection of $UO_2^{2+}$ based on colorimetric-electrochemical dual signals. The LOD for the two detection modes are as low as 107 pmol/L and 347 pmol/L, respectively.

Recent advances clearly indicate that COFs can simultaneously provide high-capacity adsorption and sensitive fluorescence-based detection of $UO_2^{2+}$ [97]. Their modular synthesis enables the integration of diverse functional groups [98], which endows them with both strong binding affinity and selective signal transduction, while their intrinsic porosity supports high sorption capacity. Importantly, fluorescent COFs combine sensitivity with reversibility [99], underscoring their potential for sustainable environmental monitoring. Nevertheless, challenges remain in scaling up synthesis and ensuring long-term stability in complex natural waters, which must be addressed for practical deployment.

### *3.4. Other Porous and Organic Materials*

Beyond MOFs and COFs, various other porous and organic matrices have also been explored for uranyl sensing, including covalent organic polymers (COPs), molecularly imprinted polymers (MIPs), and polymer–inorganic hybrids. These materials combine facile synthesis, good chemical stability, and low cost, making them attractive candidates for practical uranyl detection and enrichment. Studies on COPs illustrate their potential. Leng et al. utilized the dual advantages of COPs and polyarylene ether to synthesize three amidoxime-functionalized covalent organic polymers (bPF-AO, tBPF-AO, and tPF-AO) featuring distinct architectures through simple condensation reactions and subsequent surface treatment [100]. MIPs and hybrid systems provide further options, achieving selectivity via templated cavities or by combining organic and inorganic binding moieties. Such materials represent cost-effective and robust complements to MOFs and COFs, though their relatively limited structural precision and tunability constrain sensitivity and selectivity.

## 4. AI in Uranyl Capture and Detection

AI has been widely integrated into uranyl detection, not as a single-method solution but as a versatile enabler across multiple analytical strategies. From Raman and fluorescence spectroscopy to gamma spectrometry, electrochemical monitoring, and material discovery, AI has demonstrated its ability to enhance signal interpretation, improve detection sensitivity, and accelerate sorbent development (Figure 7).

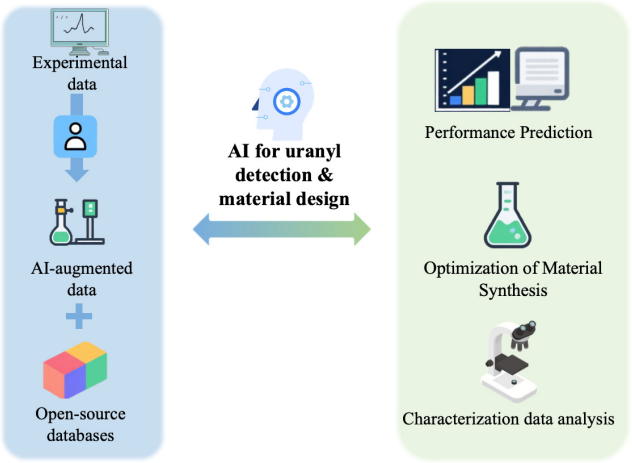


**Figure 7.** Schematic illustration of AI-enabled uranyl detection and prediction workflow.

Over the past decades, AI technologies have undergone a remarkable resurgence. Advances in classification, discriminant analysis, and neural network (NN) techniques have enabled their application in tasks ranging from isotope identification to the complex qualitative and quantitative analysis of uranium spectra [101]. Traditionally, Raman analysis has relied on pattern matching between unknown spectra and reference databases with well-characterized features, a process often hindered by the poor crystallinity or mixed phases of environmental samples. Smith et al. developed interpretable machine learning models capable of classifying uranium minerals based solely on Raman spectra, using peroxide chemistry and other physicochemical features [102]. This approach allows the generation of mineral profiles describing physical and chemical properties, enabling the rapid identification of unknown minerals without precise pattern matching to spectral libraries. Similarly, Juma Moses et al. combined laser Raman microspectroscopy with principal component analysis and multivariate curve resolution–alternating least squares to achieve size-resolved forensic analysis of uranium in nuclear aerosols [103]. Their method identified trace uranium species in aerosols, resolving three distinct bands (816 $cm^{-1}$, 854 $cm^{-1}$, and 868 $cm^{-1}$), which were deconvoluted by MCR-ALS and attributed to uranium in $PM_{4.5}$ aerosols. Machine learning has also been successfully applied to electrochemical monitoring. Jung et al. investigated cathodic potential monitoring in high-temperature electrorefining processes for nuclear safeguards [104]. Using process monitoring data and artificial neural networks, they classified normal (single-element deposition) and abnormal (binary co-deposition) states with cathodic potential as the target signal. By integrating transfer learning and recurrent neural network architectures, their model achieved up to 95% classification accuracy, highlighting its utility for efficient data-driven anomaly detection in nuclear materials processing.

Gamma spectrometry represents another area where AI integration has proven valuable. Bae et al. developed a machine learning framework to predict uranium enrichment levels from M400 CZT gamma spectra [105], using both experimental and synthetic $U_3O_8$ spectra to train fully connected neural network and convolutional neural network models. The resulting predictions achieved mean absolute errors of 0.23% and 0.099% (enrichment percentage points), respectively. Zhang et al. proposed a machine learning-based spectral analysis method tailored for high-speed logging and gamma spectra with energy drift characteristics [106]. Through parameter optimization, they constructed back-propagation neural network (BP-NN), generalized regression neural network, and support vector machine models. Among these, the BP-NN exhibited the best performance, with a mean squared error of 0.2333 and a mean absolute error of 0.1699 for uranium content quantification. Notably, the method maintained high accuracy at logging speeds up to 6 m/min, indicating its potential for overcoming speed-dependent distortions and enabling faster in-situ measurements. Chiman et al. developed a rapid framework to generate realistic mixed

 https://doi.org/10.53941/ges.2025.100014

spectra and employed the synthesized data for mixed isotope identification [107]. The study integrated traditional and state-of-the-art machine learning and deep learning algorithms. This approach was applied to predict uranium enrichment levels, demonstrating its feasibility and effectiveness in practical scenarios.

Beyond signal analysis, AI has also accelerated the design of advanced sorbent materials. By constructing structure–performance databases of MOFs, COFs, and functionalized nanocomposites, machine learning models predict adsorption capacity and selectivity toward $UO_2^{2+}$, while interpretable frameworks such as SHAP analysis elucidate the contributions of pore structure, functional groups, and electronic properties. This closed-loop paradigm, in which predictive modeling guides material selection followed by experimental validation, greatly shortens the discovery cycle for high-performance uranyl adsorbents. For instance, Wang et al. proposed a novel integrated ML framework, comprising structural decomposition, feature integration, and predictive modeling, to correlate the structures of MOFs with their gas adsorption capacity [108]. Using all available chemical and geometric features as inputs, they trained an ML model to predict the adsorption capacity of MOFs. Through two case studies focused on hydrogen storage and ethylene/ethane separation, the reliability and efficiency of the proposed ML framework for modeling MOF properties were demonstrated. These applications show that AI does not privilege any single detection method but instead provides complementary advantages across spectroscopic, radiometric, electrochemical, and material design approaches, laying the foundation for future AI-enabled multimodal platforms that combine sensitivity, selectivity, and portability for real-world uranyl monitoring.

## 5. Conclusions

Material-based platforms for uranyl detection and removal have advanced rapidly in recent years, providing diverse strategies across optical and electrochemical, and removal strategies. These approaches benefit from the unique structural and functional properties of nanoparticles, MOFs, COFs, and composite materials, which enable high sensitivity as well as selective binding and removal in complex environmental matrices. Meanwhile, the integration of AI is beginning to transform the field by improving signal interpretation, guiding data-driven material discovery, and bridging detection with remediation. However, challenges remain in ensuring reproducibility, selectivity, and stability under realistic conditions. Addressing these issues through the design of multifunctional, sustainable materials and the development of AI-enabled multimodal platforms will be essential for translating laboratory innovations into practical detection–removal tools. Such efforts will not only enhance the reliability of uranyl monitoring but also contribute to safeguarding environmental health and safety on a broader scale.

## Author Contributions

W.Z.: Writing—original draft; Z.S.: Conceptualization, Writing—review & editing; S.W.: Writing—review & editing; X.T.: Writing—review & editing; X.W.: Conceptualization, Supervision. All authors have read and agreed to the published version of the manuscript.

## Institutional Review Board Statement

Not applicable.

## Informed Consent Statement

Not applicable.

## Data Availability Statement

Not applicable.

## Conflicts of Interest

The authors declare no conflict of interest.

## Use of AI and AI-Assisted Technologies

AI-assisted tools were used only for language refinement. All scientific content was reviewed, validated, and approved by the authors, who take full responsibility for the final manuscript.

## References

1. Sun, Z.L.; Chen, Z.S.; Wang, S.H.; et al. Nuclear energy: Where next? *Innovation* **2026**, *7*, 101093.
2. Tai, X.S.; Sun, Z.L. Extra-high extraction of uranium from seawater by covalent organic frameworks through structure geometry and functional active site modification. *Sustain. Carbon. Mater.* **2025**, *1*, e006.
3. Chen, T.; Liu, T.; Zhou, L.; et al. Ternary boron carbon nitrides hollow nanotubes with tunable p-n homojunction for photo-assisted uranium extraction: A combined batch, EXAFS and DFT calculations. *Appl. Catal. B Environ.* **2022**, *318*, 121815.
4. Chen, X.T.; He, L.F.; Wang, Y.; et al. Trace analysis of uranyl ion ($UO_2^{2+}$) in aqueous solution by fluorescence turn-on detection via aggregation induced emission enhancement effect. *Anal. Chim. Acta* **2014**, *847*, 55–60.
5. Averseng, O.; Hagège, A.; Taran, F.; et al. Surface plasmon resonance for rapid screening of uranyl affine proteins. *Anal. Chem.* **2010**, *82*, 9797–9802.
6. Fukuda, S.; Ikeda, M.; Nakamura, M.; et al. Acute toxicity of subcutaneously administered depleted uranium and the effects of CBMIDA in the simulated wounds of rats. *Health Phys.* **2009**, *96*, 483–492.
7. Lourenço, J.; Pereira, R.; Gonçalves, F.; et al. Metal bioaccumulation, genotoxicity and gene expression in the

European wood mouse (*Apodemus sylvaticus*) inhabiting an abandoned uranium mining area. *Sci. Total Environ.* **2013**, *443*, 673–680.
8. Selvakumar, R.; Ramadoss, G.; Menon, M.P.; et al. Challenges and complexities in remediation of uranium contaminated soils: A review. *J. Environ. Radioact.* **2018**, *192*, 592–603.
9. Yildiz, E.; Saçmaci, S.; Kartal, S.; et al. A new chelating reagent and application for coprecipitation of some metals in food samples by FAAS. *Food Chem.* **2016**, *194*, 143–148.
10. Balaram, V. Recent advances in the determination of elemental impurities in pharmaceuticals-status, challenges and moving frontiers. *Trends Anal. Chem.* **2016**, *80*, 83–95.
11. Santos, J.S.; Teixeira, L.S.G.; dos Santos, W.N.L.; et al. Uranium determination using atomic spectrometric techniques: An overview. *Anal. Chim. Acta* **2010**, *674*, 143–156.
12. Sanyal, K.; Khooha, A.; Das, G.; et al. Direct determination of oxidation states of uranium in mixed-valent uranium oxides using total reflection X-ray fluorescence X-ray absorption near-edge spectroscopy. *Anal. Chem.* **2017**, *89*, 871–876.
13. Bings, N.H.; Bogaerts, A.; Broekaert, J.A.C. Atomic spectroscopy: A review. *Anal. Chem.* **2010**, *82*, 4653–4681.
14. Hellé, G.; Mariet, C.; Cote, G. Liquid-liquid extraction of uranium(VI) with aliquat® 336 from HCl media in microfluidic devices: Combination of micro-unit operations and online ICP-MS determination. *Talanta* **2015**, *139*, 123–131.
15. Kalita, M.P.C.; Deka, K.; Das, J.; et al. X-ray diffraction line profile analysis of chemically synthesized lead sulphide nanocrystals. *Mater. Lett.* **2012**, *87*, 84–86.
16. Ajitha, B.; Reddy, Y.A.K.; Kim, M.J.; et al. Superior catalytic activity of synthesized triangular silver nanoplates with optimized sizes and shapes. *Catal. Sci. Technol.* **2016**, *6*, 8289–8299.
17. Nasrollahzadeh, M.; Zahraei, A.; Ehsani, A.; et al. Synthesis, characterization, antibacterial and catalytic activity of a nanopolymer supported copper(II) complex as a highly active and recyclable catalyst for the formamidation of arylboronic acids under aerobic conditions. *RSC Adv.* **2014**, *4*, 20351–20357.
18. Rasheed, T.; Bilal, M.; Nabeel, F.; et al. Fluorescent sensor based models for the detection of environmentally-related toxic heavy metals. *Sci. Total Environ.* **2018**, *615*, 476–485.
19. Ullah, N.; Mansha, M.; Khan, I.; et al. Nanomaterial-based optical chemical sensors for the detection of heavy metals in water: Recent advances and challenges. *Trends Anal. Chem.* **2018**, *100*, 155–166.
20. He, W.W.; Hua, D.B. Spectrographic sensors for uranyl detection in the environment. *Talanta* **2019**, *201*, 317–329.
21. Wu, X.M.; Huang, Q.X.; Mao, Y.; et al. Sensors for determination of uranium: A review. *Trends Anal. Chem.* **2019**, *118*, 89–111.
22. Chen, Z.; Zhang, Z.Y.; Qi, J.; et al. Colorimetric detection of heavy metal ions with various chromogenic materials: Strategies and applications. *J. Hazard. Mater.* **2023**, *441*, 129889.
23. Fan, Y.J.; Li, J.W.; Guo, Y.P.; et al. Digital image colorimetry on smartphone for chemical analysis: A review. *Measurement* **2021**, *171*, 108829.
24. Hou, D.B.; Zhang, J.; Chen, L.; et al. Water quality analysis by UV-Vis spectroscopy: A review of methodology and application. *Spectrosc. Spectr. Anal.* **2013**, *33*, 1839–1844.
25. Zhang, H.Y.; Ruan, Y.J.; Lin, L.; et al. A turn-off fluorescent biosensor for the rapid and sensitive detection of uranyl ion based on molybdenum disulfide nanosheets and specific DNAzyme. *Spectrochim. Acta A* **2015**, *146*, 1–6.
26. Wang, H.P.; Chen, P.; Dai, J.W.; et al. Recent advances of chemometric calibration methods in modern spectroscopy: Algorithms, strategy, and related issues. *Trends Anal. Chem.* **2022**, *153*, 116648.
27. Pérez-Jiménez, A.I.; Lyu, D.; Lu, Z.X.; et al. Surface-enhanced Raman spectroscopy: Benefits, trade-offs and future developments. *Chem. Sci.* **2020**, *11*, 4563–4577.
28. Han, X.X.; Rodriguez, R.S.; Haynes, C.L.; et al. Surface-enhanced Raman spectroscopy. *Nat. Rev. Methods Primers* **2022**, *1*, 87.
29. Zhou, B.; Shi, L.F.; Wang, Y.S.; et al. Resonance light scattering determination of uranyl based on labeled DNAzyme-gold nanoparticle system. *Spectrochim. Acta A* **2013**, *110*, 419–424.
30. Li, S.J.; Liao, L.F.; Wu, R.R.; et al. Resonance light scattering detection of fructose bisphosphates using uranyl-salophen complex-modified gold nanoparticles as optical probe. *Anal. Bioanal. Chem.* **2015**, *407*, 8911–8918.
31. Lu, Y.Y.; Liang, X.Q.; Niyungeko, C.; et al. A review of the identification and detection of heavy metal ions in the environment by voltammetry. *Talanta* **2018**, *178*, 324–338.
32. Tang, X.; Han, H.; Li, L.; et al. Electrodes functionalized with advanced recognition materials for trace electrochemical sensing of uranyl ion. *Microchem. J.* **2024**, *199*, 109924.
33. Wang, S.S.; Zhang, J.B.; Gharbi, O.; et al. Electrochemical impedance spectroscopy. *Nat. Rev. Methods Primers* **2021**, *1*, 50.
34. Aragay, G.; Merkoçi, A. Nanomaterials application in electrochemical detection of heavy metals. *Electrochim. Acta* **2012**, *84*, 49–61.
35. Pacella, N.; DeRouin, A.; Pereles, B.; et al. Geometrical modification of magnetoelastic sensors to enhance sensitivity. *Smart Mater. Struct.* **2015**, *24*, 025018.
36. Zhang, H.; Lin, L.; Zeng, X.; et al. Magnetic beads-based DNAzyme recognition and AuNPs-based enzymatic catalysis amplification for visual detection of trace uranyl ion in aqueous environment. *Biosens. Bioelectron.* **2016**, *78*, 73–79.
37. Wu, X.M.; Mao, Y.; Wang, D.Y.; et al. Designing a colorimetric sensor containing nitrogen and oxygen atoms for uranyl ions identification: Chromatic mechanism, binding feature and on-site application. *Sens. Actuators B* **2020**, *307*, 127681.
38. Liang, Y.; He, Y. Arsenazo III-functionalized gold nanoparticles for photometric determination of uranyl ion. *Microchim. Acta* **2016**, *183*, 407–413.

39. Drogat, N.; Jauberty, L.; Chaleix, V.; et al. Sensing of the uranyl ion based on its complexation with bisphosphonate-capped gold nanoparticles. *Mater. Lett.* **2014**, *122*, 208–211.
40. Zhang, D.Y.; Chen, Z.; Omar, H.; et al. Colorimetric peroxidase mimetic assay for uranyl detection in sea water. *ACS Appl. Mater. Interfaces* **2015**, *7*, 4589–4594.
41. Saha, A.; Neogy, S.; Rao, D.R.M.; et al. Colorimetric and visual determination of ultratrace uranium concentrations based on the aggregation of amidoxime functionalized gold nanoparticles. *Microchim. Acta* **2019**, *186*, 183.
42. Zhang, L.S.; Huang, D.S.; Zhao, P.X.; et al. Colorimetric detection for uranyl ions in water using vinylphosphonic acid functionalized gold nanoparticles based on smartphone. *Spectrochim. Acta A* **2022**, *269*, 120748.
43. Xu, Y.L.; Wei, J.H.; Chen, X.W. Visible light-responsive sulfone-based covalent organic framework as metal-free nanoenzyme for visual colorimetric determination of uranium. *Chemosensors* **2022**, *10*, 248.
44. Xiao, S.J.; Huang, J.; Qiu, A.T.; et al. Advanced "turn-on" colorimetric uranium platform based on the enhanced nanozyme activity of a donor-acceptor structured covalent organic framework. *Anal. Chim. Acta* **2024**, *1302*, 342503.
45. Amini, A.; Khajeh, M.; Oveisi, A.R.; et al. A porous multifunctional and magnetic layered graphene oxide/3D mesoporous MOF nanocomposite for rapid adsorption of uranium(VI) from aqueous solutions. *J. Ind. Eng. Chem.* **2021**, *93*, 322–332.
46. Bai, F.; Yang, X.; Yang, C.; et al. Amidoxime covalent organic framework@$Fe_3O_4$ based magnetic solid-phase extraction for rapid and sensitive determination of trace uranium in seafood. *J. Chromatogr. A* **2025**, *1740*, 465564.
47. Zhang, J.J.; Cheng, F.F.; Li, J.J.; et al. Fluorescent nanoprobes for sensing and imaging of metal ions: Recent advances and future perspectives. *Nano Today* **2016**, *11*, 309–329.
48. Saha, A.; Debnath, T.; Neogy, S.; et al. Micellar extraction assisted fluorometric determination of ultratrace amount of uranium in aqueous samples by novel diglycolamide-capped quantum dot nanosensor. *Sens. Actuators B* **2017**, *253*, 592–602.
49. Liu, W.; Dai, X.; Bai, Z.L.; et al. Highly sensitive and selective uranium detection in natural water systems using a luminescent mesoporous metal-organic framework equipped with abundant lewis basic sites: A combined batch, X-ray absorption spectroscopy, and first principles simulation investigation. *Environ. Sci. Technol.* **2017**, *51*, 3911–3921.
50. Liu, W.; Dai, X.; Wang, Y.L.; et al. Ratiometric monitoring of thorium contamination in natural water using a dual-emission luminescent europium organic framework. *Environ. Sci. Technol.* **2019**, *53*, 332–341.
51. Wang, Z.; Xu, C.; Lu, Y.X.; et al. Microplasma electrochemistry controlled rapid preparation of fluorescent polydopamine nanoparticles and their application in uranium detection. *Chem. Eng. J.* **2018**, *344*, 480–486.
52. Zhang, Z.; Zhang, D.; Shi, C.; et al. 3,4-Hydroxypyridinone-modified carbon quantum dot as a highly sensitive and selective fluorescent probe for the rapid detection of uranyl ions. *Environ. Sci. Nano* **2019**, *6*, 1457–1465.
53. Zheng, Z.J.; Zhang, L.; Wang, L.Z.; et al. Ultrasensitive detection of $UO_2^{2+}$ based on dopamine-functionalized MoOx quantum dots. *Luminescence* **2022**, *37*, 127–133.
54. Ghosh, M.; Swain, K.K.; Singh, P.K. Thioflavin-T incorporated cerium-ATP coordination polymer nanoparticles: A promising system for detection of uranyl ion ($UO_2^{2+}$) in aqueous medium. *Langmuir* **2023**, *39*, 7017–7028.
55. Chen, X.F.; Mei, Q.S.; Yu, L.; et al. Rapid and on-site detection of uranyl ions via ratiometric fluorescence signals based on a smartphone platform. *ACS Appl. Mater. Interfaces* **2018**, *10*, 42225–42232.
56. Feng, T.T.; Zhao, S.L.; Cao, M.; et al. Highly sensitive and specific uranyl ion detection by a fluorescent sensor containing uranyl-specific recognition sites. *Sci. Bull.* **2025**, *70*, 70–77.
57. Stiles, P.L.; Dieringer, J.A.; Shah, N.C.; et al. Surface-enhanced raman spectroscopy. *Annu. Rev. Anal. Chem.* **2008**, *1*, 601–626.
58. Sharma, B.; Frontiera, R.R.; Henry, A.I.; et al. SERS: Materials, applications, and the future. *Mater. Today* **2012**, *15*, 16–25.
59. Gai, T.; Jiang, J.L.; Wang, S.F.; et al. Photoreduced $Ag^+$/sodium alginate supramolecular hydrogel as a sensitive SERS membrane substrate for rapid detection of uranyl ions. *Anal. Chim. Acta* **2024**, *1316*, 342826.
60. Gai, T.; Jiang, J.L.; Wang, S.F.; et al. Highly sensitive and selective determination of uranyl ions based on Ag/ $Ag_2O$-COF composite SERS substrate. *Talanta* **2024**, *277*, 126407.
61. Wang, S.F.; Zou, S.M.; Yang, S.L.; et al. $HfO_2$-wrapped slanted Ag nanorods array as a reusable and sensitive SERS substrate for trace analysis of uranyl compounds. *Sens. Actuators. B. Chem.* **2018**, *265*, 539–546.
62. Jiang, J.L.; Ma, L.W.; Chen, J.; et al. SERS detection and characterization of uranyl ion sorption on silver nanorods wrapped with $Al_2O_3$ layers. *Microchim. Acta* **2017**, *184*, 2775–2782.
63. He, X.; Wang, S.F.; Liu, Y.; et al. Ultra-sensitive detection of uranyl ions with a specially designed high-efficiency SERS-based microfluidic device. *Sci. China Chem.* **2019**, *62*, 1064–1071.
64. Wang, N.; Du, J.J.; Li, X.; et al. Magnetic MOF substrates for the rapid and sensitive surface-enhanced raman scattering detection of uranyl. *Anal. Chem.* **2023**, *95*, 12956–12963.
65. Sun, C.M.; Dong, W.R.; Peng, J.X.; et al. Dual-mode fluorescence-SERS sensor for sensitive and selective detection of uranyl ions based on satellite $Fe_3O_4$-Au@CdTe nanostructure. *Sens. Actuators. B. Chem.* **2020**, *325*, 128644.
66. Wang, S.F.; Jiang, J.L.; Wu, H.X.; et al. Self-assembly of silver nanoparticles as high active surface-enhanced Raman scattering substrate for rapid and trace analysis of uranyl(VI) ions. *Spectrochim. Acta A* **2017**, *180*, 23–28.
67. Jiang, J.L.; Wang, S.F.; Deng, H.; et al. Rapid and sensitive detection of uranyl ion with citrate-stabilized silver nanoparticles by the surface-enhanced Raman scattering technique. *R. Soc. Open Sci.* **2018**, *5*, 181099.

68. Yuan, C.; Ge, H.W.; Cao, B.M.; et al. SERS detection of uranyl based on MOF-coated gold nanooctahedron hybrid. *Anal. Sci.* **2024**, *40*, 2111–2116.
69. Lu, W.; Band, B.S.F.; Yu, Y.; et al. Resonance light scattering and derived techniques in analytical chemistry: Past, present, and future. *Microchim. Acta* **2007**, *158*, 29–58.
70. Shang, L.; Chen, H.J.; Deng, L.; et al. Enhanced resonance light scattering based on biocatalytic growth of gold nanoparticles for biosensors design. *Biosens. Bioelectron.* **2008**, *23*, 1180–1184.
71. Zhou, B.; Wang, Y.S.; Yang, H.X.; et al. A sensitive resonance light scattering assay for uranyl ion based on the conformational change of a nuclease-resistant aptamer and gold nanoparticles acting as signal reporters. *Microchim. Acta* **2014**, *181*, 1353–1360.
72. Shrivastava, A.; Sharma, J.; Soni, V. Various electroanalytical methods for the determination of uranium in different matrices. *Bull. Fac. Pharm. Cairo Univ.* **2013**, *51*, 113–129.
73. Zhou, Z.P.; Zhou, Y.M.; Liang, X.Z.; et al. Electrochemical sensor for uranium monitoring in natural water based on poly Nile blue modified glassy carbon electrode. *J. Solid. State Electrochem.* **2022**, *26*, 1139–1149.
74. Ghoreishi, S.M.; Behpour, M.; Mazaheri, S.; et al. Uranyl sensor based on a N,N'-bis(salicylidene)-2-hydroxy-phenylmethanediamine and multiwall carbon nanotube electrode. *J. Radioanal. Nucl. Chem.* **2012**, *293*, 201–210.
75. Li, Y.J.; Wang, Z.M.; Liu, C.; et al. Graphene oxide modified $H_4$L-ion imprinting electrochemical sensor for the detection of uranyl ions. *Z. Anorg. Allg. Chem.* **2021**, *647*, 1914–1920.
76. Zhou, Z.P.; Zhou, Y.M.; Liang, X.Z.; et al. Sensitive detection of uranium in water samples using differential pulse adsorptive stripping voltammetry on glassy carbon electrode. *J. Radioanal. Nucl. Chem.* **2019**, *322*, 2049–2056.
77. Wen, Y.; Sun, Y.C.; Liu, Y.T.; et al. Green synthesis of 2% g-$C_3N_4$/$SnS_2$-V3/$CQD_1$ composite photocatalyst from waste plant soot for efficient U(VI) removal: Mechanistic insights. *Chem. Eng. J.* **2024**, *494*, 153247.
78. Guo, Y.X.; Liu, H.W.; Cao, H.; et al. Complexation of uranyl with benzoic acid in aqueous solution at variable temperatures: Potentiometry, spectrophotometry and DFT calculations. *Dalton Trans.* **2023**, *52*, 11265–11271.
79. Xie, X.; Tian, Y.; Qin, Z.; et al. Complexation of manganese with glutarimidedioxime: Implication for extraction uranium from seawater. *Sci. Rep.* **2017**, *7*, 43503.
80. Akl, Z.F.; Ali, T.A. A novel modified screen-printed electrode with triazole surfactant assembled on silver nanoparticles for potentiometric determination of uranium. *J. Radioanal. Nucl. Chem.* **2017**, *314*, 1865–1875.
81. Yang, M.; Liao, L.F.; Zhang, G.L.; et al. Detection of uranium with a wireless sensing method by using salophen as receptor and magnetic nanoparticles as signal-amplifying tags. *J. Radioanal. Nucl. Chem.* **2013**, *298*, 1393–1399.
82. Sun, Z.L.; Chen, Z.S.; Tai, X.S.; et al. Uranium extraction from seawater: Methods and challenges. *Sci. China Chem.* **2025**, *68*, 3923–3926.
83. Wei, G.; Chen, Z.S.; Tai, X.S.; et al. Recent progress of uranium extraction and its catalytic applications. *Trans. Tianjin Univ.* **2025**, *31*, 390–402.
84. Sun, Z.L.; Liao, Y.; Zhang, Y.Y. Sustainable carbon materials in environmental and energy applications. *Sustain. Carbon. Mater.* **2025**, *1*, e007.
85. Wang, Z.; Lu, Y.X.; Yuan, H.; et al. Microplasma-assisted rapid synthesis of luminescent nitrogen-doped carbon dots and their application in pH sensing and uranium detection. *Nanoscale* **2015**, *7*, 20743–20748.
86. Sun, Z.L.; Wang, X.K. Covalent metal-organic frameworks: Emerging star materials for seawater uranium harvesting. *Sci. Sin. Chim.* **2025**, *55*, 1–2.
87. Liang, L.Y.; Qin, F.P.; Wang, S.; et al. Overview of the materials design and sensing strategies of nanopore devices. *Coord. Chem. Rev.* **2023**, *478*, 214998.
88. Lu, Y.F.; Yu, L.; Zhang, S.L.; et al. Dual-functional fluorescent metal-organic framework based beads for visual detection and removal of oxytetracycline in real aqueous solution. *Appl. Surf. Sci.* **2023**, *625*, 157202.
89. Jin, K.; Lee, B.; Park, J. Metal-organic frameworks as a versatile platform for radionuclide management. *Coord. Chem. Rev.* **2021**, *427*, 213473.
90. Sun, Y.F.; Yu, L.; Wu, K.L.; et al. Non-rare earth doped metal-organic framework for fluorescent detection of uranyl in real seawater. *Sens. Actuators. B. Chem.* **2025**, *436*, 137643.
91. Wang, Y.; Xing, S.H.; Zhang, X.; et al. A family of functional Ln-organic framework constructed by iodine-substituted aromatic polycarboxylic acid for turn-off sensing of $UO_2^{2+}$. *Appl. Organomet. Chem.* **2019**, *33*, e4898.
92. Cao, X.H.; Sun, Y.B.; Wang, Y.C.; et al. PtRu bimetallic nanoparticles embedded in MOF-derived porous carbons for efficiently electrochemical sensing of uranium. *J. Solid. State Electrochem.* **2021**, *25*, 425–433.
93. Niu, C.P.; Zhang, C.R.; Cui, W.R.; et al. A conveniently synthesized redox-active fluorescent covalent organic framework for selective detection and adsorption of uranium. *J. Hazard. Mater.* **2022**, *425*, 127951.
94. Zhen, D.S.; Liu, C.L.; Deng, Q.H.; et al. Novel olefin-linked covalent organic framework with multifunctional group modification for the fluorescence/smartphone detection of uranyl ion. *ACS Appl. Mater. Interfaces* **2024**, *16*, 27804–27812.
95. Guo, X.T.; Wang, X.Y.; Wen, S.Z.; et al. Silver nanoparticle-grafted amidoxime covalent organic framework: A Highly sensitive and selective SERS substrate for uranium detection in natural water systems. *Adv. Funct. Mater.* **2025**, *35*, 2500901.
96. Chen, Z.J.; Liu, J.Q.; Wang, W.Y.; et al. Aptamer-regulated colorimetric and electrochemical dual-mode sensor for the detection of uranyl ions utilizing AuNCs@COF composite. *Microchim. Acta* **2025**, *192*, 295.
97. Lu, H.; Fu, D.; Tai, X.S.; et al. Metal-organic frameworks/covalent-organic frameworks-based materials in organic/inorganic pollutant elimination and $CO_2$ reduction applications. *ChemNanoMat* **2025**, *11*, e202500244.

98. Qian, H.L.; Wang, Y.; Yan, X.P. Covalent organic frameworks for environmental analysis. *Trends Anal. Chem.* **2022**, *147*, 116516.
99. Zhao, Y.; Yan, Y.; Wu, Z.; et al. A novel fluorescent covalent organic framework for the selective detection of fluoride ion. *J. Mater. Sci.* **2022**, *57*, 13425–13432.
100. Leng, R.; Sun, Y.C.; Wang, C.Z.; et al. Design and fabrication of hypercrosslinked covalent organic adsorbents for selective uranium extraction. *Environ. Sci. Technol.* **2023**, *57*, 9615–9626.
101. Kangas, L.J.; Keller, P.E.; Siciliano, E.R.; et al. The use of artificial neural networks in PVT-based radiation portal monitors. *Nucl. Instrum. Methods Phys. Res., Sect. A* **2008**, *587*, 398–412.
102. Smith, R.; Spano, T.L.; McDonnell, M.; et al. Interpretable machine learning models classify minerals via spectroscopy. *Sci. Rep.* **2025**, *15*, 15807.
103. Wabwile, J.M.; Angeyo, H.K.; Massop, A.D. Exploring band-free Raman microspectrometry combined with PCA and MCR-ALS for size-resolved forensic analysis of uranium in aerosols in a model nuclear atmosphere. *J. Environ. Radioact.* **2023**, *270*, 107295.
104. Jung, Y.E.; Ahn, S.K.; Yim, M.S. Investigation of neural network-based cathode potential monitoring to support nuclear safeguards of electrorefining in pyroprocessing. *Nucl. Eng. Technol.* **2022**, *54*, 644–652.
105. Bae, J.W.; Hu, J.W. Machine learning framework for predicting uranium enrichments from M400 CZT gamma spectra. *Nucl. Instrum. Methods Phys. Res. Sect. A* **2024**, *1068*, 169705.
106. Zhang, Y.; Ye, Y.J.; Qiu, J.; et al. Study on quantitative interpretation of uranium spectral gamma-ray logging based on machine learning algorithm. *Nucl. Eng. Technol.* **2024**, *56*, 4959–4965.
107. Kwan, C.; Ayhan, B.; Stavola, A.; et al. A fast framework for generating radioactive mixture dpectra and its application to remote high-performance mixture identification. *Electronics* **2025**, *14*, 1688.
108. Wang, Z.H.; Zhou, Y.G.; Zhou, T.; et al. Identification of optimal metal-organic frameworks by machine learning: Structure decomposition, feature integration, and predictive modeling. *Comput. Chem. Eng.* **2022**, *160*, 107739.